Significant photoinduced Kerr rotation achieved in semiconductor microcavities

R. V. Cherbunin,[1] M. Vladimirova,[2] K. V. Kavokin,[1,3] A. V. Mikhailov,[1]
N. E. Kopteva,[1] P. G. Lagoudakis,[4] and A. V. Kavokin[1,4]
[1]*Spin Optics Laboratory, St-Petersburg State University, 1, Ulianovskaya, St-Peterbsurg 198504, Russia*
[2]*Laboratoire Charles Coulomb, UMR 5221 CNRS/Université Montpellier 2, F-34095 Montpellier, France*
[3]*Ioffe Physical-Technical Institute of the RAS, 26, Politechnicheskaya, 194021 St-Petersburg, Russia*
[4]*Department of Physics & Astronomy, University of Southampton, Southampton SO17 1BJ, United Kingdom*
(Received 5 October 2014; revised manuscript received 17 February 2015; published 18 May 2015)

Giant Kerr rotation and ellipticity are observed and investigated in an asymmetric planar microcavity with a quantum well in the active region. Rotation angle of the polarization plane as well as ellipticity were determined from time- and frequency-resolved measurements of the Stokes vector components of reflected light. It was found that in a small range of the cavity mode detunings the polarized pump pulse creates a large splitting of the lower polariton branch while leaving its linewidth almost the same. This fact gives a possibility to observe at such detunings the Kerr rotation angle and ellipticity, close to their extremes. A theoretical analysis shows that the decisive role in reaching extreme polarization rotation angles is played by the structure asymmetry. Comprehensive analysis of the polarization state of the light in this regime shows that both renormalization of the exciton energy and the saturation of the excitonic resonance contribute to the observed optical nonlinearities.

DOI: 10.1103/PhysRevB.91.205308 PACS number(s): 71.36.+c, 42.65.Hw

I. INTRODUCTION

Semiconductor microcavities elate an increasing interest, due to their capacity to enhance the light-matter interaction [1–4]. In particular, Kerr (Faraday) rotation, that is the rotation of the polarization of light upon reflection (transmission) from a media characterized by a nonzero magnetization projection to the direction of light propagation, can be increased by orders of magnitude by placing the spin polarized quasiparticles in a high quality factor planar optical microcavity [5–11]. Using this approach, spectacular effects, such as Kerr rotation by a single electron spin in a quantum dot and Kerr rotation by nuclear spins, were recently observed [12,13]. Various protocols for quantum nondemolition measurements based on a quantum dot embedded in a microcavity have been proposed [14,15]. Amplification of the electron spin noise, an effect measured via fluctuations of the Faraday rotation, was also achieved by placing a two-dimensional electron gas in a microcavity [16].

In the reflection geometry, the cavity-induced enhancement of the Kerr rotation is not only due to the enhanced interaction between light and matter. An important role plays an abrupt change of the phase of reflected light when crossing the photon mode resonance [17]. By engineering the cavity mirrors, an interferometer with infinite phase slope can be designed, although the intensity of the reflected light will be zero at this point. While the Kerr rotation angle, which is determined by the slope of the phase dependence on the optical frequency, will be large in this case, the amplitude of the measured signal, which is defined by both amplitude and phase, will be very small [18,19].

The spectral behavior of the phase of the light wave reflected from a Fabry-Pérot resonator with a highly reflecting back mirror (which is typically the case for semiconductor microcavities) is known to be determined by the way in which the reflected wave is formed. Generally, it is contributed by the wave reflected from the front mirror and by the wave leaking from the cavity. Besides, their relative weights depend on the relationship between losses in the cavity and the front mirror reflectivity. At very low resonator losses, a standing wave of large amplitude forms inside the cavity, giving rise to an intense leakage wave. At the resonance frequency, its amplitude exceeds the amplitude of a directly reflected wave by a factor of 2, while their phases are opposite. In this case the spectral dependence of the reflection phase is monotonous, with the phase changing from 0 to 2π in crossing the resonance. If absorption in the cavity is strong, then the amplitude of the standing wave is small, the leakage wave is weak, and the reflected wave is formed mainly by the front mirror. In this case, the role of the cavity in light reflection from the structure is insignificant. With respect to the phase, this means that it does not change by 2π when passing the resonance, and the spectrum of the reflection phase has the shape of the derivative of the Lorentz contour with a small magnitude. In between these two extreme cases, there exists a certain level of losses at which the leakage wave and directly reflected wave at the resonance have equal amplitudes and opposite phases. In this case reflection at the resonance frequency completely disappears, but the derivative from the reflection phase on the frequency goes to infinity. This regime is called the regime of impedance matching (IM), because all the incident power is absorbed in the cavity [19].

In spite of the obvious importance of this effect, it was, to the best of our knowledge, rarely addressed when working with semiconductor microcavities. In Ref. [20] a principle of electric control over the phase of reflected light was proposed, based on energy level shifts in a double-quantum-well structure placed in a microcavity that resulted in modulation of losses in the cavity. In Ref. [21] Kerr rotation changed its spectral shape under heating of the microcavity structure from 4 to 150 K from a single peak at low temperature to a bipolar structure, resembling the Lorentz derivative, at about 100 K. This effect was partly explained by variation of light absorption by density-of-state tails in mirrors, which could change relative contributions of directly reflected and leakage

waves. But determination of the formation mechanisms of Kerr rotation was complicated in this case by widening and further disappearing of the exciton resonance at high temperatures. Finally, in our work peculiarities of the spin-noise optical spectra were observed and analyzed near the IM point of a microcavity [16].

Kerr and Faraday rotation angles are determined by circular birefringence (gyrotropy) of the active media inside the cavity. In the case of the quantum wells embedded into the cavity, strong coupling between excitons and the cavity mode leads to the formation of new quasiparticles called exciton polaritons [1–4]. In such structures, under circularly polarized optical pumping, photoinduced gyrotropy, and therefore Kerr rotation is determined by the excitonic component of polaritons. The excitonic fraction in the polariton depends on the detuning between exciton and photon modes, and is given by the Hopfield coefficient [2]. Polariton-polariton interactions responsible for the photoinduced Kerr rotation are governed by the excitonic fraction in the polariton, and can be identified as a shift of the exciton energy and saturation of the exciton absorbtion. Nevertheless, their dependence on spin, exciton-photon detuning, and pumping power is still a subject of the debate [22–30]. It is well established, however, that strong optical pumping leads to the saturation of the excitonic transition followed by the transition towards weak coupling regime and dissociation of the exciton. Thus, this transition limits the photoinduced Kerr rotation in polaritonic systems at high powers. The values of order of 10 deg has been reported in the literature, much less than $\pi/2$, a theoretical limit for the rotation of the polarization plane in reflection geometry (Kerr rotation) [8,10]. The reason for that is the lack of the IM, which ensure maximum enhancement of the photoinduced gyrotropy. To achieve this regime the absorbtion in the cavity should be sufficiently low. That is why when a QW is placed in a microcavity and a strong coupling regime is achieved, resonant absorbtion of the polariton modes makes the IM condition difficult to fulfill. To optimize photoinduced Kerr rotation in a QW microcavity a trade-off between maximum excitonic effects and minimum absorbtion should be found, by designing the structure where the cavity mode is slightly below the QW exciton resonance at the IM point.

In this work we demonstrate photoinduced Kerr rotation close to the theoretical maximum of $\pi/2$ in a QW microcavity operating in the strong coupling regime, and elucidate the role of the IM in this effect. A careful analysis of the polarization state of the reflected light allows for the identification and quantitative analysis of the microscopic mechanisms responsible for the enhanced gyrotropy of microcavities under optical pumping. Both spin-dependent blue shift of the exciton energy and the reduction of the exciton oscillator strength are shown to contribute to the photoinduced Kerr rotation on equal footing.

II. EXPERIMENT

The sample under study is grown on GaAs substrate and consists of a 1λ cavity with a 20-nm quantum well in the center. It is sandwiched between two Bragg mirrors, the front (rear) mirror consists of 15 (25) pairs of $\lambda/4$ AlAs/$Al_{0.1}Ga_{0.9}As$ layers. The cavity is grown on a wedge, so that the exciton cavity detuning can be controlled by choosing the laser spot (of 50 μm radius) position on the sample surface. The sample was not specially grown for this work and its design is further detailed in Refs. [31,32]. The calculated transmission of the front mirror ($t_1 = 0.017$) is chosen to compensate the below-band-gap residual absorption of the $Al_{0.1}Ga_{0.9}As$ layers, forming the mirror and the cavity. Such a condition ensures the deepest minima in reflection spectra at low temperatures and zero detuning between the cavity mode and heavy hole exciton.

The sample is placed in a closed-cycle optical cryostat at 4.2 K and investigated in the reflection geometry using the time-resolved pump-probe technique. The gyrotropy in the active layer is created by optical pumping with circularly polarized pulses of a mode-locked Ti:sapphire laser operating at 76 MHz, resonant with the upper polariton branch. From the broad spectrum of the femtosecond laser pulse, pump pulses characterized by the spectral width of 0.1 meV are cut by an acousto-optic filter, the time-integrated pump power varied in the range of 0–20 mW. Because the reflection coefficient on the upper polariton branch strongly depends on the detuning, in the quantitative analysis we use absorbed optical power rather than the incident power, assuming that all the power transmitted through the front mirror is absorbed in the QW. Probe pulses are 20-meV wide and linearly polarized in the vertical plane parallel to the crystallographic axis (110) to minimize the influence of the optical anisotropy of the sample. The time-integrated power does not exceed 0.1 mW. The polarization state of the probe beam is analyzed using an ellipsometer. It consists of two phase plates (with half-wave and quarter-wave retardation) and a linear polarizer, placed one after another in front of the entrance slit of a 0.5-m spectrometer equipped with a CCD camera.

For a given delay between pump and probe pulses, the spectra of the reflected probe were recorded in six polarizations: vertical, horizontal, diagonal, antidiagonal, right circular, and left circular. These spectra provide the state of polarization of the probe beam in terms of the Stokes vector components, which can be mapped to the Poincare sphere:

$$S_{\mu\nu} = (I_\mu - I_\nu)/(I_\mu + I_\nu), \tag{1}$$

where $I_{\mu,\nu}$ is the intensity of light components polarized along horizontal ($\mu = H$) and vertical ($\nu = V$) axes, diagonal (rotated by $\pi/4$) axes: $\mu = D$, $\nu = A$, and of the circularly polarized components: $\mu = \sigma+$, $\nu = \sigma-$.

The Kerr rotation angle ϕ and ellipticity Θ are obtained from the Stokes parameters:

$$\varphi = 0.5 \begin{cases} \arctan\frac{y}{x} & \text{if } x > 0, \\ \arctan\frac{y}{x} + \pi & \text{if } y \geqslant 0,\ x < 0, \\ \arctan\frac{y}{x} - \pi & \text{if } y < 0,\ x < 0, \end{cases} \tag{2}$$

where $y = S_{DA}$, $x = S_{VH}$, and

$$\Theta = \arcsin(S_{\sigma+\sigma-}). \tag{3}$$

Figure 1 shows a color map of the linear reflectivity (in the absence of the pump) as a function of the photon energy and x coordinate on the sample surface. The energy of the cavity mode shifts linearly across the sample. For each position, three dips in the spectrum are observed, corresponding to the cavity photon mode (MC mode), heavy hole (X), and light hole

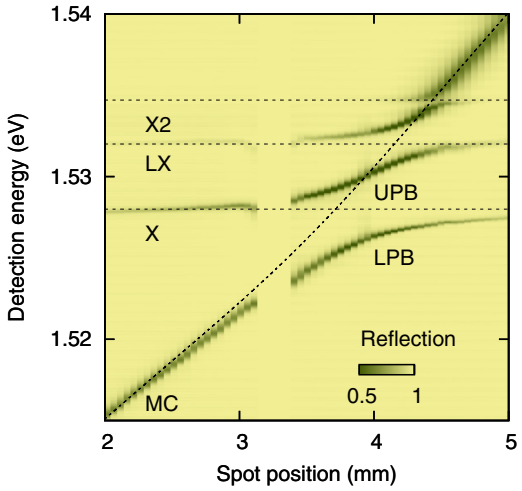

FIG. 1. (Color online) Reflection spectrum of the structure as a function of position in the structure plane.

(LX) exciton. Both X and LX modes show anticrossings with the MC mode. The highest energy anticrossing is due to the second quantized state of the exciton in the QW (X2). Above the anticrossing point with the upper exciton level, the MC mode width becomes several times larger due to the interband absorption in the QW and increased losses in the mirrors. These linear reflectivity spectra are described in the framework of the nonlocal dielectric response model. The reflection coefficient of the cavity in the absence of pumping is given by the function $r(\omega)$, obtained by summation of waves reflected from all the heterointerfaces [11],

$$r(\omega) = 1 + \frac{2t_1^2}{t_1^2 + t_2^2} \frac{i\Gamma}{\omega_c - \omega - i(\Gamma + \Gamma_s) - G},$$

$$G = \sum_{j=1}^{3} \frac{g_j^2}{\omega_j - \omega - i\Gamma_j}. \quad (4)$$

TABLE I. Exciton parameters for fitting of the reflection spectrum. Photon mode parameters: $t_1/t_2 = 4.35$, $\Gamma_s = 5\ \mu$eV.

Transition	ω_j (meV)	Γ_j (meV)	g_j (meV)
Heavy exciton, X	1528.0	0.3	1.8
Light exciton, LH	1532.0	0.3	1.4
Upper level exciton, X2	1534	0.3	0.5

Here ω_c is the cavity eigenfrequency, Γ (Γ_s) are rates of radiative (nonradiative) decay of the cavity mode, g_j is the strength of coupling between the exciton and the light field (equal to one half of the Rabi frequency [2]), ω_j is the exciton resonance frequency in the quantum well, and Γ_j is the exciton damping rate. The index j spans over three exciton resonances, X, LX, and X2. The mirrors are characterized by the transmission coefficients t_1 and t_2 for the front and rear mirrors, respectively. The inhomogeneous broadening of the cavity resonance due to the gradient of the cavity width under the light spot has been taken into account via convolution of the amplitude reflection coefficient $r(\omega)$ with the Gaussian distribution of the width Γ_{inh}.

The parameters obtained by fitting this model to the linear reflectivity spectra are summarized in Table I. The IM is achieved in this structure at the MC mode detuning $\simeq -3$ meV. Note that due to the inhomogeneous broadening, the reflectivity does not go to zero at the LPB energy even at IM. Although LX and X2 polaritons do not induce strong photoinduced Kerr rotation, it is mandatory to take them into account in the modeling of the spectra, for the correct description of the polariton states.

Figures 2(a)–2(f) shows the effect of the σ^+-polarized pumping on the polarization-resolved probe reflectivity spectra. Measurements are taken in the vicinity of low polariton branch at $\Delta = -3$ meV. For each polarization of detection, the dependence of the normalized reflectivity on the detection energy and on the pump-probe delay is represented as a 2D

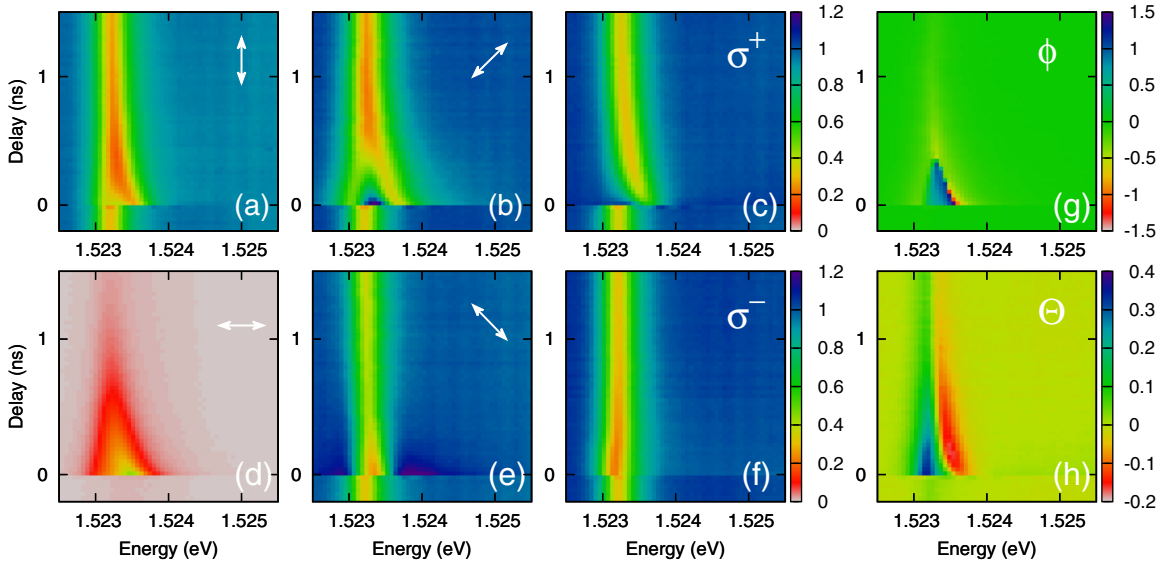

FIG. 2. (Color online) (a)–(f) Kinetics of the reflection spectra in six polarization of detection: vertical, diagonal, right circular, horizontal, antidiagonal, and left circular. Cavity detuning $\Delta = -3$ meV, absorbed pump power 1 mW. (g) and (h) Kerr rotation angle φ and ellipticity angle Θ calculated from (a)–(f) as a function of detection energy and pump-probe delay.

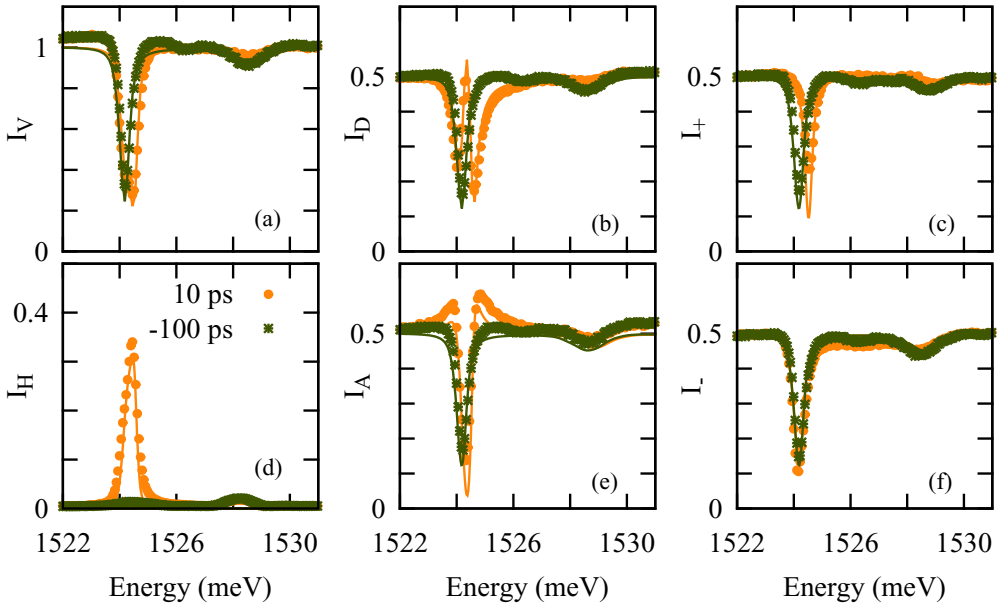

FIG. 3. (Color online) Reflectivity spectra of the probe for different detection polarizations. Cavity detuning $\Delta = -3$ meV, σ^+-polarized pump power is $P \simeq 1$ mW. Spectra taken at -100 ps pump-probe delay (unperturbed system, green symbols) are compared with the photoinduced spectra measured at 10 ps pump-probe delay (orange symbols). Lines show the results of the modeling.

color map. At negative delays the spectral dip corresponding to the LPB is observed in all polarizations, except cross linear (I_H), where reflectivity is zero. At positive delays, a circularly polarized pump induces a blue shift of the low polariton branch in cocircular (I_+) and red shift in the countercircular I_H polarization. In vertical and diagonal polarizations, I_V, I_H, pump effect manifests itself rather as a splitting of the polariton mode. In horizontal (cross linear with the probe) polarization of detection, I_H, strong reflectivity is induced by the pump. The Kerr rotation and ellipticity obtained from reflection spectra are shown in Figs. 2(g) and 2(h), respectively. In the following we will limit the discussion to the fixed pump-probe delay. For such analysis we compare two spectra for each polarization: the spectrum at negative delay, which is identical to the spectrum of probe in the absence of the pump, and the spectrum at the pump-probe delay of 10 ps (Fig. 3). Studies of the polarization dynamics and relaxation are beyond the scope of this paper and will be reported elsewhere.

It is instructive to represent the pump-induced polarization state extracted from the polarization-resolved measurements (Fig. 3) in terms of the Stokes vector hodograph upon variation of the probe energy. In Figs. 4(a) and 4(b) two different detunings of the photon mode are shown, $\Delta \simeq -3$ meV, corresponding to IM, and $\Delta \simeq -5$ meV, that is above IM. Figure 4(a) shows the Stocks vector projection on the equatorial (S_{HV},S_{DA}) plane. In this representation, the Kerr rotation angle φ is readily visualized as the deviation of the Stokes vector S from the abscissae. Arrows indicate maximum photoinduced rotation angle $\varphi_{\max}$ reached at this power and detuning. The projection on the vertical plane (S_{HV},$S_{\sigma\sigma}$), containing the initial polarization of the incident probe beam, is shown in Fig. 4(b), its deviation from the vertical axis (S_{+-}) yields the ellipticity angle θ. The arrows show the elipticity at the energy of the maximum Kerr rotation.

The maximum values of the Kerr rotation angle measured for each pumping power are shown by symbols in Fig. 4(c). For $\Delta \simeq -5$ meV, $\varphi_{\max} < \pi/2$ the power dependence of Kerr rotation is monotonic. This means that the hodograph of the Stokes vector never turns around zero [as in Fig. 4(c), red circles], even at the maximum pumping power. By contrast, at $\Delta \simeq -3$ meV, it crosses zero at the absorbed power of about 0.5 mW [Fig. 4(c), green squares]. This means, that at this pumping intensity, when moving across the probe spectrum, the Stocks vector hodograph crosses zero in the equatorial plane, and then returns back. The rotation of $\pi/2$ appears as a discontinuity since the angle between initial and rotated polarization planes is defined in the $[-\pi/2,\pi/2]$ interval, according to Eq. (2).

III. MODEL

To reproduce the energy, power, and detuning dependence of the photoinduced gyrotropy, we employ a simple phenomenological model. We assume that the effect of the optical pumping can be described in terms of the blue shift of the X resonance (i) and reduction of coupling with the MC mode in the cocircular polarization (ii) [8]. Both effects are supposed to be linearly dependent on the absorbed power P or, equivalently, on the polariton density. The importance of the latter contribution has been evidenced previously [24], but it can often be neglected [27,28]. Including not only the energy shift but also the reduction of the coupling is mandatory for the correct description of the experimental data. The resulting energy of the X state under cocircular pumping can be written as $\hbar\omega_X(P) = \hbar\omega_X(0) + \hbar\delta\omega_X P$, and the X-MC coupling parameter as $g_X(P) = g_X(0) + \delta g_X P$. Pumping in the countercircular polarization is supposed to induce no noticeable variation of the excitonic parameters at negative detuning, because interaction between polaritons with

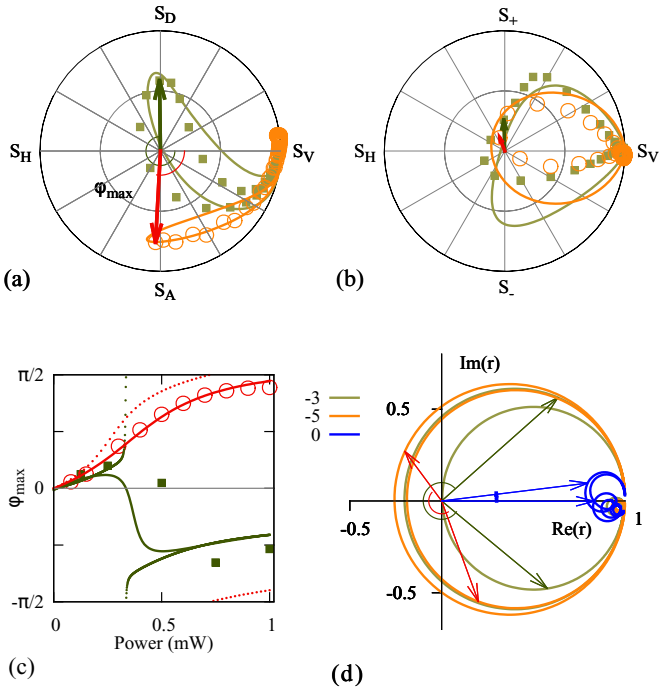

FIG. 4. (Color online) (a) Projection of the reflected probe Stocks vector spectrum on the equatorial plane of a Poincare sphere. Orange circles: $\Delta = -5$ meV, $P = 0.4$ mW, green triangles: $\Delta = -3$ meV, $P = 1$ mW. Lines : modeling. Energy range is the same as in Fig. 3. (b) The same in the vertical plane of the Poincare sphere (ellipticity angle). (c) Maximum rotation angle as a function of pump power for $\Delta = -5$ meV and $\Delta = -3$ meV. Symbols show the experimental data, dashed lines show modeling taking into account inhomogeneous broadening of the cavity mode, and dotted lines stand for the model without inhomogeneous broadening. (d) Calculated function $r(\omega)$ on the complex plane for co- (dashed line) and cross- (solid line) circular polarizations of detection for $\Delta = -5$ meV (orange), -3 meV (green), and 0 meV (blue). The angle between two arrows indicates the maximum Kerr rotation angle at each detuning.

opposite spins is negligibly weak in this case [27,28]. The resulting reflection coefficients for right- (r^+) and left-circular (r^-) polarizations of light can be calculated as functions of power using Eq. (4) with power-dependent exciton energy and exciton-cavity coupling in the cocircular polarization. This is sufficient to model the experimental data: the photoinduced reflectivity signal in any polarization, Stocks vector of the reflected light, and the power dependence of the Kerr rotation angle. The results of the fitting to the measured Stocks vector components and Kerr rotation angle are shown by solid lines in Figs. 4(a)–4(d), while the row spectra in six different polarizations are shown in Fig. 3. Two fitting parameters $\delta\omega_X = 0.5$ meV/mW and $\delta g_X = 0.4$ meV/mW are used to reproduce the ensemble of the photoinduced effects. One can see that this simple model reproduces quite well the experimental data. Note that the inhomogeneous broadening Γ_{inh} plays an important role here. Indeed, dotted lines in Fig. 4(c) show the Kerr rotation angle which one could expect for the same cavity parameters but assuming $\Gamma_{\text{inh}} = 0$. A much sharper increase of the Kerr angle in the vicinity of $\pi/2$ point could be expected in this case. Moreover, the depolarization of the probe is entirely due to the inhomogeneous broadening, and the polarization degree would not be affected by the pumping in the homogeneous system.

IV. DISCUSSION

It is now possible to elucidate the role of the impedance matching condition in the optically induced gyrotropy. For this purpose we plot in a complex plane r^+ calculated at the same power as in Fig. 4(a) and r^- which does not depend on power for three different values of the cavity detuning, Fig. 4(d). While the frequency passes through the cavity resonance, the function $r(\omega)$ makes a circle on the complex plane, starting from real unity and eventually coming back. The radius of this circle equals unity in the system with zero absorbtion, but in a realistic system it is determined by the absorption in the cavity, and thus is sensitive to the detuning of the MC mode from the X resonance. The complex reflection coefficient circumvents zero point at $\Delta \simeq -5$ meV (above IM), but not at $\Delta \simeq 0$ (below IM), the reflectivity turns to zero at $\Delta \simeq -3$ meV, corresponding to the IM. Cocircular pumping shifts the system towards more negative detuning, due to the photoinduced modification of the excitonic transition energy, so that the radius of the circle increases (dashed circles), and the reflectivity vector shifts along this circle across the spectrum. The reflectivity vectors corresponding to the maximum Kerr rotation are indicated by arrows. They are obtained from the fitting of the data for three different detuning values. One can see that below IM at zero detuning the rotation is indeed very small. The maximum rotation is obtained at $\Delta \simeq -3$ meV, where the system is pushed above IM by optical pumping. However, at $\Delta \simeq -5$ meV, further above IM, Kerr angle is reduced again. This is the consequence of weaker excitonic effects at stronger negative detunings, and thus smaller polariton shifts.

The power dependence of upper (E_{UPB}) and lower (E_{LPB}) polariton energy shifts measured in co- and countercircular polarizations are shown in Fig. 5 for two different detunings. One can see that polariton shifts are essentially linear in density, which justifies the assumptions of the model (lines). At both values of the detuning, LPB experiences the blue shift, while the shift of E_{UPB} is negative at $\Delta = -5$ meV and positive at $\Delta = -3$ meV. This behavior is due to the combination of two excitonic nonlinearities, exciton energy shift and oscillator strength decrease. In contrast with the experiments of Ref. [28], where LPB shifts achieved at the most negative detuning of $\Delta = -2$ meV do not exceed 0.1 meV, here stronger LPB shifts indicate higher polariton densities, and thus the additional mechanism (exciton oscillator strength decrease) coming into play. We roughly estimate that the saturation density in our sample $n_{\text{sat}} = 10^{11}$ cm^{-2} corresponds to the absorbed power $P = 280$ W cm^{-2}. According to Ref. [24], polariton nonlinear dynamics is governed by the renormalization of the exciton energy only for carrier densities below $0.04 n_{\text{sat}}$. Above this critical density the phase space filling leading to the reduction of the exciton oscillator strength cannot be neglected. This justifies our approach, where taking into account both exciton energy shift and oscillator strength decrease is mandatory, to account for the ensemble of the experimental observations.

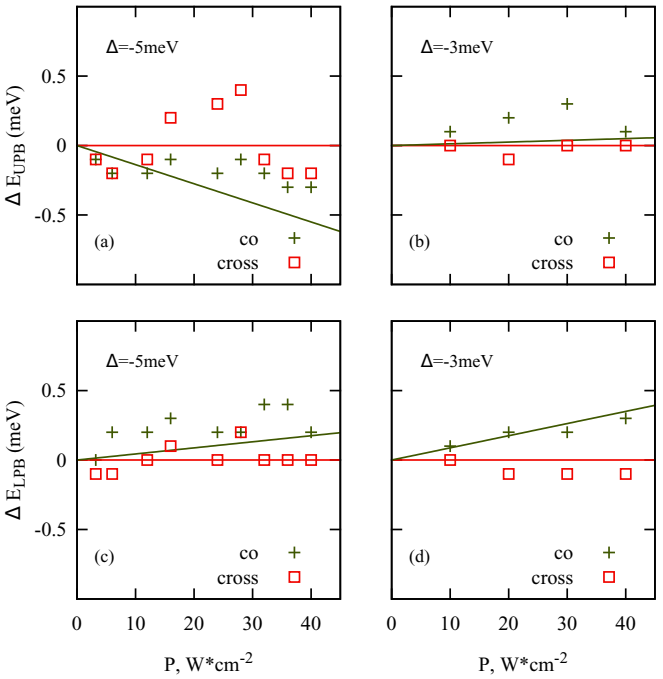

FIG. 5. (Color online) Photoinduced energy shifts of the upper and lower polariton branches in co- (black crosses) and cross- (red squares) circular polarization of detection. (a) and (c) $\Delta = -5$ meV. (b) and (d) $\Delta = -3$ meV. Lines are the corresponding energy shifts obtained by the fit.

Our results clearly show that the studied structure, though demonstrating large photoinduced Kerr effect, is not optimal with respect to Kerr sensitivity or maximum possible rotation. The improved Kerr sensitivity, i.e., the ability to reach considerable rotations under smaller pump powers, is what one should look for, aiming at technical applications. In the optimized structures, the optical control over polarization of the reflected beam could be reached with maximum efficiency. To this end, the photonic mode should be placed at negative detuning, so as to put the system above the IM. At the same time, the exciton resonance should be made as narrow as possible, which would enhance the nonlinearity mechanism based on Zeeman shifts of exciton sublevels. This would require growing high-quality quantum wells (QWs). Besides, wider QWs may prove advantageous. At the same time, increasing the exciton-photon coupling by, e.g., using multiple QWs, is not expected to improve the sensitivity. Further optimization of the structure with respect to the maximum Kerr angles may be reached by designing an exactly impedance-matched structure. But this design has an obvious disadvantage of low total reflectivity at the optical resonance, which would diminish the intensity of the output light and eventually reduce the efficiency of optical control instead of increasing it.

V. CONCLUSIONS

In conclusion, we have demonstrated the photoinduced Kerr rotation angle in a semiconductor microcavity of up to $\pi/2$ rad. The conditions which ensure maximum Kerr rotation constitute a trade-off between the needs to maximize photoinduced excitonic effects (polarization-dependent blue shift and oscillator strength reduction) close to zero cavity mode detuning, and minimize the absorption in order to achieve the IM. Understanding of the major role played by IM is crucial for the design of specific samples, e.g., suitable for giant amplification of the optical gyrotropy. These results open the way for realization of fast optical polarization modulators operating at zero magnetic field.

ACKNOWLEDGMENTS

This work was partially supported by the Russian Ministry of Education and Science (Contract No. 11.G34.31.0067 with SPbSU) and by RFBR in the frame of International Collaborative Research Center TRR 160. The authors acknowledge Saint-Petersburg State University for a research grant 11.38.213.2014. R.V.C. thanks RFBR project No. 14-02-31846 for financial support. M.V. acknowledges EU INDEX PITN-GA-2011-289968 and LABEX NUMEV AAP 2013-1-006.

[1] C. Weisbuch, M. Nishioka, A. Ishikawa, and Y. Arakawa, Phys. Rev. Lett. **69**, 3314 (1992).
[2] A. Kavokin, J. Baumberg, G. Malpuech, and F. Laussy, *Microcavities*, Series on Semiconductor Science and Technology (Oxford University Press, Oxford, 2007).
[3] B. Deveaud, ed., *The Physics of Semiconductor Microcavities* (Wiley-VCH, New York, 2007).
[4] V. Timofeev and D. Sanvitto, eds., *Springer Series in Solid-State Sciences* (Springer, New York, 2012).
[5] A. V. Kavokin, M. R. Vladimirova, M. A. Kaliteevski, O. Lyngnes, J. D. Berger, H. M. Gibbs, and G. Khitrova, Phys. Rev. B **56**, 1087 (1997).
[6] M. Haddad, R. André, R. Frey, and C. Flytzanis, Solid State Commun. **111**, 61 (1999).
[7] C. Gourdon, G. Lazard, C. Testelin, E. Ivchenko, J. Aaviksoo, and G. Karczewski, Phys. Status Solidi A **190**, 431 (2002).
[8] D. Pereda Cubian, M. Haddad, R. André, R. Frey, G. Roosen, J. L. Arce Diego, and C. Flytzanis, Phys. Rev. B **67**, 045308 (2003).
[9] J.-T. Liu and K. Chang, Appl. Phys. Lett. **90**, 061114 (2007).
[10] A. Brunetti, M. Vladimirova, D. Scalbert, R. André, D. Solnyshkov, G. Malpuech, I. A. Shelykh, and A. V. Kavokin, Phys. Rev. B **73**, 205337 (2006).
[11] C. Y. Hu, A. Young, J. L. O'Brien, W. J. Munro, and J. G. Rarity, Phys. Rev. B **78**, 085307 (2008).
[12] C. Arnold, V. Loo, A. Lemaître, I. Sagnes, O. Krebs, P. Voisin, P. Senellart, and L. Lanco, Phys. Rev. X **4**, 021004 (2014).
[13] R. Giri, S. Cronenberger, M. M. Glazov, K. V. Kavokin, A. Lemaître, J. Bloch, M. Vladimirova, and D. Scalbert, Phys. Rev. Lett. **111**, 087603 (2013).
[14] R.-B. Liu, W. Yao, and L. J. Sham, Phys. Rev. B **72**, 081306 (2005).

[15] S. Puri, P. L. McMahon, and Y. Yamamoto, Phys. Rev. B **90**, 155421 (2014).
[16] S. V. Poltavtsev, I. I. Ryzhov, R. V. Cherbunin, A. V. Mikhailov, N. E. Kopteva, G. G. Kozlov, K. V. Kavokin, V. S. Zapasskii, P. V. Lagoudakis, and A. V. Kavokin, Phys. Rev. B **89**, 205308 (2014).
[17] C. Gourdon, G. Lazard, V. Jeudy, C. Testelin, E. Ivchenko, and G. Karczewski, Solid State Commun. **123**, 299 (2002).
[18] J. H. Chow, I. C. Littler, D. S. Rabeling, D. E. McClelland, and M. B. Gray, Opt. Express **16**, 7726 (2008).
[19] D. S. Rabeling, J. H. Chow, M. B. Gray, and D. E. McClelland, Opt. Express **18**, 9314 (2010).
[20] B. Pezeshki, G. A. Williams, and J. S. Harris, Appl. Phys. Lett. **60**, 1061 (1992).
[21] G. Salis and M. Moser, Phys. Rev. B **72**, 115325 (2005).
[22] M. Kuwata-Gonokami, S. Inouye, H. Suzuura, M. Shirane, R. Shimano, T. Someya, and H. Sakaki, Phys. Rev. Lett. **79**, 1341 (1997).
[23] P. G. Lagoudakis, P. G. Savvidis, J. J. Baumberg, D. M. Whittaker, P. R. Eastham, M. S. Skolnick, and J. S. Roberts, Phys. Rev. B **65**, 161310 (2002).
[24] A. Huynh, J. Tignon, Ph. Roussignol, C. Delalande, R. André, R. Romestain, and D. Le Si Dang, Phys. Rev. B **66**, 113301 (2002).
[25] P. Renucci, T. Amand, X. Marie, P. Senellart, J. Bloch, B. Sermage, and K. V. Kavokin, Phys. Rev. B **72**, 075317 (2005).
[26] Z. Vörös, D. W. Snoke, L. Pfeiffer, and K. West, Phys. Rev. Lett. **103**, 016403 (2009).
[27] M. Vladimirova, S. Cronenberger, D. Scalbert, K. V. Kavokin, A. Miard, A. Lemaître, J. Bloch, D. Solnyshkov, G. Malpuech, and A. V. Kavokin, Phys. Rev. B **82**, 075301 (2010).
[28] N. Takemura, S. Trebaol, M. Wouters, M. T. Portella-Oberli, and B. Deveaud, Phys. Rev. B **90**, 195307 (2014).
[29] C. Adrados, A. Amo, T. C. H. Liew, R. Hivet, R. Houdré, E. Giacobino, A. V. Kavokin, and A. Bramati, Phys. Rev. Lett. **105**, 216403 (2010).
[30] M. M. Glazov, H. Ouerdane, L. Pilozzi, G. Malpuech, A. V. Kavokin, and A. D'Andrea, Phys. Rev. B **80**, 155306 (2009).
[31] R. Rapaport, E. Cohen, A. Ron, E. Linder, and L. N. Pfeiffer, Phys. Rev. B **63**, 235310 (2001).
[32] P. G. Lagoudakis, M. D. Martin, J. J. Baumberg, A. Qarry, E. Cohen, and L. N. Pfeiffer, Phys. Rev. Lett. **90**, 206401 (2003).